



UNIVERSIDADE ESTADUAL DE CAMPINAS  
SISTEMA DE BIBLIOTECAS DA UNICAMP  
REPOSITÓRIO DA PRODUÇÃO CIENTÍFICA E INTELLECTUAL DA UNICAMP

**Versão do arquivo anexado / Version of attached file:**

Versão do Editor / Published Version

**Mais informações no site da editora / Further information on publisher's website:**

<https://academic.oup.com/jge/article/11/5/055001/5110292>

**DOI: 10.1088/1742-2132/11/5/055001**

**Direitos autorais / Publisher's copyright statement:**

©2014 by Oxford University Press. All rights reserved.

DIRETORIA DE TRATAMENTO DA INFORMAÇÃO

Cidade Universitária Zeferino Vaz Barão Geraldo

CEP 13083-970 – Campinas SP

Fone: (19) 3521-6493

<http://www.repositorio.unicamp.br>

# A methodology to calibrate water saturation estimated from 4D seismic data

Alessandra Davolio, Célio Maschio and Denis José Schiozer

Department of Petroleum Engineering, FEM, UNICAMP/CEPETRO, São Paulo, Brazil

E-mail: [davolio@dep.fem.unicamp.br](mailto:davolio@dep.fem.unicamp.br)

Received 18 March 2014, revised 12 August 2014

Accepted for publication 21 August 2014

Published 12 September 2014

## Abstract

Time-lapse seismic data can be used to estimate saturation changes within a reservoir, which is valuable information for reservoir management as it plays an important role in updating reservoir simulation models. The process of updating reservoir properties, history matching, can incorporate estimated saturation changes qualitatively or quantitatively. For quantitative approaches, reliable information from 4D seismic data is important. This work proposes a methodology to calibrate the volume of water in the estimated saturation maps, as these maps can be wrongly estimated due to problems with seismic signals (such as noise, errors associated with data processing and resolution issues). The idea is to condition the 4D seismic data to known information provided by engineering, in this case the known amount of injected and produced water in the field. The application of the proposed methodology in an inversion process (previously published) that estimates saturation from 4D seismic data is presented, followed by a discussion concerning the use of such data in a history matching process. The methodology is applied to a synthetic dataset to validate the results, the main of which are: (1) reduction of the effects of noise and errors in the estimated saturation, yielding more reliable data to be used quantitatively or qualitatively and (2) an improvement in the properties update after using this data in a history matching procedure.

Keywords: 4D seismic data, saturation estimation, volume calibration, history matching, reservoir simulation

(Some figures may appear in colour only in the online journal)

## Nomenclature

|                      |  |                  |   |
|----------------------|--|------------------|---|
| LHM                  | local history matching   | V <sub>b</sub>   | volume of a grid block  |
| IP                   | P-impedance  | nb               | number of grid blocks   |
| IS                   | S-impedance  | CF               | volume correction factor  |
| Sw                   | water saturation   | Bw               | water formation volume factor                                     |
| Sw <sub>c</sub>      | connate water saturation   | SE               | simple error  |
| So <sub>r</sub>      | residual oil saturation  | QE               | quadratic error   |
| P                    | pore pressure  |                  |   |
| P <sub>ProdMin</sub> | minimum pore pressure (producer wells)                                 | <b>Subscript</b> |   |
| P <sub>InjMax</sub>  | maximum pore pressure (injector wells)                                 | <i>seis</i>      | parameter derived from 4D seismic data                            |
| Δ <sub>4D</sub>      | time-lapse difference operator   | <i>sim</i>       | parameter computed from reservoir simulation results              |
| V <sub>inj</sub>     | volume of injected water (standard conditions)                         | <i>base</i>      | parameter computed from the simulation results of the base model  |
| V <sub>prod</sub>    | volume of produced water (standard conditions)                         | <i>seis_cali</i> | parameter derived from 4D seismic data with the volume calibrated |
| V <sub>current</sub> | current volume of water present in the reservoir (standard conditions) | <i>t0</i>        | parameter corresponding to the base survey                        |
| φ                    | porosity   |                  |   |

## 1. Introduction

Time-lapse seismic data is an important source of information for reservoir monitoring because it provides a better understanding of the variations of dynamic properties in the reservoir. This valuable information can be used to update reservoir simulation models, which are an important tool for reservoir management (optimization strategy and planning infill drillings). Several works in the literature show successful use of 4D seismic data [2, 11, 22].

The integration between 4D seismic data and reservoir simulation is a topic of intense research. Several approaches can be used, from qualitative interpretation of 4D seismic anomalies [11, 24], which are incorporated into reservoir simulation models, to quantitative use of 4D seismic data in history matching procedures. For the latter, different approaches in the literature use different optimization algorithms. Gosselin *et al* [9] have presented a tool based on a gradient-type algorithm to perform history matching which incorporates seismic impedances and production data in the objective function. Brito *et al* [3] showed an application of this tool in the Marlim field, which showed advantages of applying an assisted process compared with traditional manual history matching. Landa and Horne [14] also used a gradient-type optimization procedure to history match production data and interpreted maps of changes in pressure and in saturation from 4D seismic data. Stephen *et al* [21] and Landa and Kumar [15] used probabilistic approaches with different sampling algorithms; the former, the Monte Carlo algorithm and the latter, the Neighborhood Algorithm (NA). Jin *et al* [12] compared three stochastic methods: Very Fast Simulating Annealing (VSA), Particle Swarm Optimization (PSO) and NA. Algorithms based on Ensemble Kalman Filter theory also solve the problem within a probabilistic approach; Skjervheim *et al* [20] and Emerick and Reynolds [8] are examples of this.

Concerning the type of data used to integrate reservoir simulation and 4D seismic data, there are three possible domains of integration: (1) amplitude, (2) impedance and (3) saturation and pressure domains.

This work focuses on the integration in the saturation and pressure domain; therefore we need to estimate these properties from seismic amplitudes or impedances. We can use different methodologies to estimate saturation and pressure changes from 4D seismic attributes [4, 5, 16–18]. They differ according to the type of seismic attribute used to estimate the dynamic changes and how the data is manipulated to obtain these estimations. These methodologies could be used to any field that holds enough seismic data (pre-stack data is usually needed for base and monitor surveys). However, challenges remain concerning seismic signal related problems (such as noise, tuning and uncertainties in rock properties and modeling).

One way of extracting more reliable information from time-lapse seismic signals is to use engineering data (well production profiles, reservoir simulation data). Engineering data, such as reservoir simulation results, are used in forward modeling for feasibility studies, or to help interpret 4D seismic

anomalies. However, few works effectively use this type of information to constrain the estimations of dynamic properties from 4D seismic data. The work of Huang *et al* [10] follows this idea; in their work they demonstrated that well production data (predominantly used for history matching) can be used to enhance the 4D seismic interpretation without the need of a reservoir model. Their methodology uses frequently repeated seismic surveys and correlates changes in the mapped seismic attributes directly to the fluid volumes injected and produced from the wells. Some ambiguities related to the interpretation of 4D signals in three different fields were clarified when using this methodology.

Toinet *et al* [23] also used engineering data to constrain 4D seismic data. The authors used a workflow to perform a 4D pre-stack inversion constrained by a range of variations of elastic properties computed from reservoir simulation results. Reservoir model information was also included as a constraint to help locate water-bearing sands more accurately. Davolio *et al* [6] also presented a methodology that uses reservoir simulation results to constrain dynamic properties estimation from 4D seismic data; this work uses the constraints, extracted from several models realizations, in a petro-elastic inversion that estimates saturation and pressure from seismic impedances, not in a pre-stack inversion as Toinet *et al* [23] did.

The present work also uses engineering information to constrain the estimation of dynamic properties from 4D seismic data. Specifically, it proposes a methodology to correct the volume of water associated with the estimated saturation maps from 4D seismic data based on the known volume of injected and produced water in the field. This calibration is important, especially when employing a quantitative use of these properties in a history matching procedure, because inputting poor estimates may lead to incorrect model updating. The proposed volume calibration can be applied to saturation maps estimated from 4D seismic data through any of the previously mentioned techniques. This work uses saturation maps estimated by the 4D petro-elastic inversion constrained to flow conditions proposed by Davolio *et al* [6]. After analyzing the results, we discuss the importance of this type of information used as input in a history matching procedure. To validate and demonstrate the benefits of this methodology, the results are shown with synthetic data.

## 2. Methodology

Water injection is commonly used to enhance oil recovery in petroleum fields. There are two main objectives when using this technique; first, to control reservoir pressure which decreases with oil production, and second, to improve sweep efficiency. However, monitoring the water flood along the reservoir is a challenge. This monitoring is very important to plan infill drillings as well as defining production strategies, in this sense 4D seismic data is helpful and can be used to estimate water saturation changes from time-lapse differences of seismic attributes. The quality of these estimations can suffer

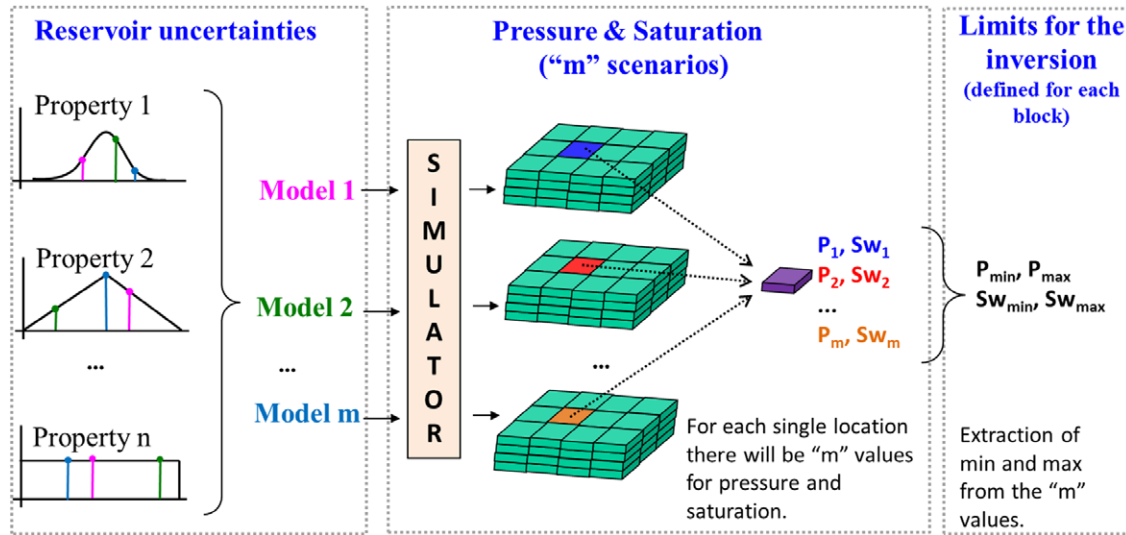


**Figure 1.** General procedure used to define outer limits of pressure and saturation for each reservoir block. ‘Property 1’, ‘Property 2’ and ‘Property n’ are generic representations of the reservoir uncertainties. ‘Model 1’, ‘Model 2’ and ‘Model m’ are generic reservoir models, generated from the combination of the reservoir uncertainties (adapted from Davolio *et al* [6]).

from seismic signal related problems (such as noise, tuning and uncertainties in rock properties and modeling). One way of minimizing this is to use knowledge available from engineering to constrain, or calibrate, the information provided by 4D seismic data. The amount of water injected in a field is such an example and is used in the methodology proposed in this work.

The methodology aims to calibrate the volume of injected water associated with the water saturation ( $Sw$ ) maps provided by 4D seismic data with the known volume of injected and produced water. To do that, we apply a multiplicative correction factor to the  $Sw$  map to calibrate it, and then we verify if the updated  $Sw$  values belong to a feasible range. This range is the key point of the calibration procedure and we estimate it from multiple reservoir simulations, according to the methodology described in Davolio *et al* [6].

Figure 1, shows more details about the range calculation. The procedure starts by defining the ‘ $n$ ’ uncertainties, or the ‘ $n$ ’ most important uncertainties of the reservoir such as porosity, absolute permeability, relative permeability, fault transmissibility and fluid properties. Then, probability density functions are attributed for each uncertainty based on knowledge available at the current characterization stage. These ‘ $n$ ’ properties are then sampled and combined to generate ‘ $m$ ’ simulation model realizations. The next section details the definition of uncertainties, sampling and combination performed in this work.

The ‘ $m$ ’ models are simulated and for each reservoir block, the range of possible values for each cell is defined by extracting the minimum and maximum  $Sw$  value along all the ‘ $m$ ’ possibilities; this range ( $[Sw_{min}, Sw_{max}]$ ) is assigned to the monitor seismic survey. It is assumed that there is a base survey acquired in the pre-production period and a monitor survey acquired after some years of production. Figure 1 shows that the same procedure can be applied for pressure.

However, only the  $Sw$  limits are needed to calibrate the volume of water.

After estimating the range  $[Sw_{min}, Sw_{max}]$  for every grid block of the model, the volume calibration can be performed as described below:

- (1) Compute the amount of injected water (in reservoir conditions) present in 4D seismic data according to equation (1):

$$V_{inj_{seis}} = \sum_{i=1}^{nb} \phi_i Vb_i (\Delta_{4D} Sw_{seis})_i, \quad (1)$$

where  $nb$  is the number of blocks of the model,  $\phi$  is the porosity,  $Vb$  is the block volume,  $\Delta_{4D} Sw_{seis}$  is the time-lapse difference of water saturation estimated from 4D seismic data.

- (2) Compute the correction factor ( $CF$ ) according to equation (2):

$$CF = V_{inj_{seis}} / V_{current}, \quad (2)$$

being that  $V_{current}$  is the current volume of water:

$$V_{current} = (V_{inj} - V_{prod}) B_w, \quad (3)$$

where  $V_{inj}$  is the known volume of injected water and  $V_{prod}$  is the known volume of produced water.  $B_w$  is the water formation volume factor which is defined as water and dissolved gas volume at reservoir conditions divided by water volume at standard conditions; it is used to convert the volume of water from surface to reservoir conditions.

- (3) Set  $i = 1$ ;
- (4) While  $i \leq nb$  calculates the calibrated water saturation value for the  $i$ th block by applying the correction factor:

$$(\Delta_{4D} Sw_{seis, cal})_i = (\Delta_{4D} Sw_{seis})_i / CF. \quad (4)$$

(5) Compute the calibrated Sw for the monitor survey:

$$(S_{w_{seis\_cali}})_i = (A_{4D} S_{w_{seis\_cali}})_i + (S_{w_{i0}})_i ; \quad (5)$$

where  $S_{w_{i0}}$  is the water saturation value at the initial time (base survey).

(6) Verify if the calibrated Sw belongs to the feasible range:

$$(S_{w_{min}})_i \leq (S_{w_{seis\_cali}})_i \leq (S_{w_{max}})_i . \quad (6)$$

(7) If inequality 6 holds, then the value of the current reservoir block (*i*th block) is set by equation (5), set  $i = i + 1$  and return to step 4; else go to step 8.

(8) If  $(S_{w_{min}})_i > (S_{w_{seis\_cali}})_i$  then  $(S_{w_{seis\_cali}})_i = (S_{w_{min}})_i$ , set  $i = i + 1$  and return to step 4, else go to step 9.

(9) If  $(S_{w_{max}})_i < (S_{w_{seis\_cali}})_i$  then  $(S_{w_{seis\_cali}})_i = (S_{w_{max}})_i$ , set  $i = i + 1$  and return to step 4.

Steps 2–9 are repeated until a satisfactory volume calibration is reached, namely  $CF - 1 < \text{tolerance}$ . Steps 1–9 are applied to the whole reservoir or to reservoir zones independently.

Some assumptions are to be considered when applying the methodology proposed above:

- 4D seismic data are at the same scale of the reservoir simulation model. For real data, an upscaling/downscaling procedure is needed to convert data from seismic to flow simulation scale.
- A 4D base survey was acquired in the pre-production period, so that the time-lapse difference of saturation provides information about the volume of injected water.
- The methodology was designed for cases where there are only connate and injected water in the reservoir, i.e., in cases where there is aquifer influx the procedure needs to be adapted.

### 3. Dataset description

To evaluate the results of the proposed methodology, all data used in this work are synthetic, as described in the following sections.

#### 3.1. Reference model

In a real problem, the data needed to apply the proposed methodology are: water saturation maps extracted from 4D seismic data, the reservoir simulation model and the multiple model realizations resulting from a combination of uncertainties process. This work uses a synthetic dataset, so, apart from the simulation model (called base<sup>1</sup> model) and the multiple realizations, another model (called reference model) that represents the true earth model is used to validate the results. Therefore, the static properties (such as porosity and permeability) and dynamic properties (such as pressure and saturation) of the reference model represent the answer that the processes should reach. Thus, the closer the

<sup>1</sup> Base model represents the model available to the engineer, namely the model that needs to be matched. There is no relation between the name ‘base’ used in this case and the ‘base survey’ that represents the first seismic acquisition in agreement with the traditional nomenclature used in geophysics.

estimated Sw map (from 4D seismic data) is to the simulation result of the reference model, the more accurate it is. Similarly, when history matching is applied, the closer the updated static properties are to those of the reference model, the better. Besides validating the results, the reference model is also used to generate the 4D seismic data as explained in the next section.

The synthetic dataset represents a sand reservoir that was discretized in a corner-point grid with  $90 \times 110 \times 5$  blocks, 60m in the *x* and *y* direction ( $5400 \times 6600$ m) and 15 m (on average) in the *z* direction. The reservoir has four faults and is drained by eight vertical producer wells, which are supported by seven water injectors (figure 2(a)); the producer wells are completed at the three top layers and the injectors at the three bottom layers (figure 2(e)). The static grid properties (porosity and permeability) were generated through a geostatistical tool (Sequential Gaussian Simulation). Figures 2(a) and (b) show the reference model static properties and figures 2(c) and (d) show the dynamic changes after 6 years of production computed through a black-oil simulator (CMG—Imex).

#### 3.2. Synthetic seismic generation

The synthetic seismic data used in this work were generated from the reference simulation model. Seismic impedances (IP and IS) were created by forward modeling through a petro-elastic model imputing the reference model properties: porosity, pressure and saturations (figure 2). No seismic amplitudes were generated, so no elastic inversion was performed to compute the impedances. All the simulation models in this work use the same grid as the reference model, so the synthetic seismic data and the simulation models are at the same scale.

We used the unconsolidated sand model [19] to calculate the dry bulk and shear moduli of the rock frame, and then used the Gassmann’s equations to compute the rock saturated moduli. The fluids moduli and density were computed through the usual Batzle and Wang [1] relations. More details and the equations definition are given in Davolio *et al* [6]. Figure 3 shows the behavior of computed seismic velocities that generate the seismic impedances. The vertical lines indicate the range of effective pressure used to compute the seismic impedances. These velocities were computed assuming a 100% brine-saturated rock with a porosity of 0.2.

The seismic dataset has four volumes of impedances, P and S impedances for two surveys (pre-production and 6 years of production).

Independent random noise of 1% of the average was added to each P and S impedance 3D volume to have more realistic synthetic data. Then a 2D median filter was applied to the noisy impedance volumes to remove the high frequency effect observed in the time-lapse differences as well as to deform the 4D anomalies but keep their general aspect. Figure 4 shows the time-lapse difference for the synthetic attributes generated before and after disturbance. Because of the median filter application, the perturbation observed in the impedances show different magnitudes for each reservoir location ranging from 1% to 50%, as shown in figure 5.

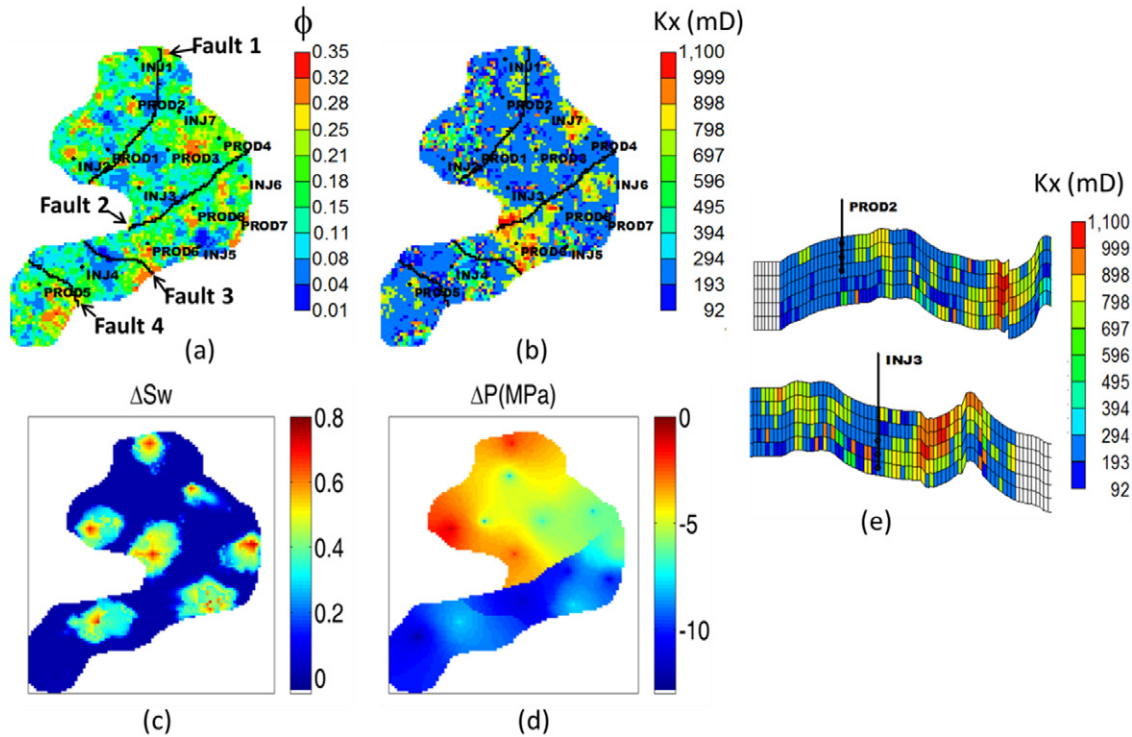


**Figure 2.** Reference reservoir model. Static properties: (a) porosity and (b) horizontal permeability. Time-lapse changes computed through a black-oil simulator: (c) water saturation and (d) pore pressure. (e) Vertical section highlighting the well completions; the grid is colored with the horizontal permeability values.

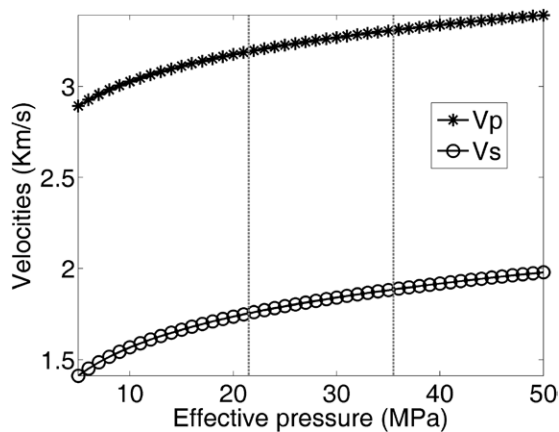


**Figure 3.** Computed seismic velocities against effective pressure. Vertical lines indicate the range of effective pressure used to compute the seismic impedances.

The noisy seismic impedances displayed in figures 4(c) and (d) were used as input of the inversion procedure used to estimate the water saturation for this dataset. The details are described in section 4.1.

### 3.3. Reservoir uncertainties

Reservoir static properties can be classified as global or local. Changes in global properties affect the flow behavior of the whole reservoir (or of a large area of it). The latter has a local effect, i.e. local changes affect local flow (e.g. around a well).

Here, global uncertainties are: fault transmissibility, relative permeability (represented by the Corey exponent, see Lake [13]) and permeability ratio (vertical/horizontal). The local uncertainties are porosity and horizontal permeability.

These uncertainties are the only differences between the reference model and all the other simulation models in this work.

The second part of this work focuses on the use of a Sw map to update the reservoir model's properties through a history matching process, i.e., the static properties of the base model are updated based on the observed dynamic properties change (Sw map) We propose to use this information to update static properties locally, following the history matching methodology in Davolio *et al* [7]. However, before running a local matching, global uncertainties need to be calibrated. This work uses a pre-calibrated (global matching) dataset, as described by Davolio *et al* [7]. Therefore, we assume only local properties (porosity and horizontal permeability) as uncertainties.

We used the Sequential Gaussian Simulation technique (SGS) to generate 200 realizations of porosity. Each porosity field was later used as a second variable for the SGS to generate 200 realizations of permeability (figure 6). To generate these images we kept constant geostatistical parameterization such as variogram, mean and standard deviation, so each image is a geostatistical realization of the SGS. We used each pair of images to generate 200 simulation models. Thus, there was no need to sample or combine the uncertainties to generate the model realizations, as each model represents a geostatistical realization of porosity and permeability.

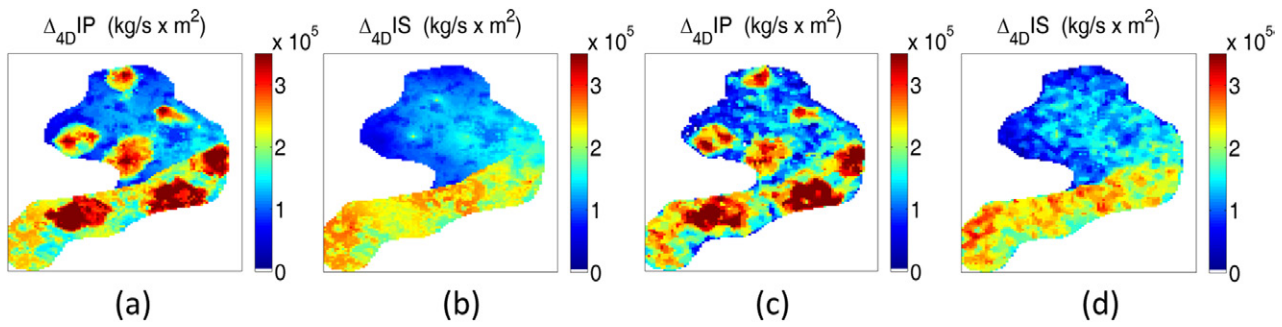


**Figure 4.** Time-lapse difference of the synthetic seismic attributes without adding noise: (a) P-impedance. (b) S-impedance. Time-lapse difference of the synthetic seismic attributes after noise addition: (c) P-impedance. (d) S-impedance. Layer 3.

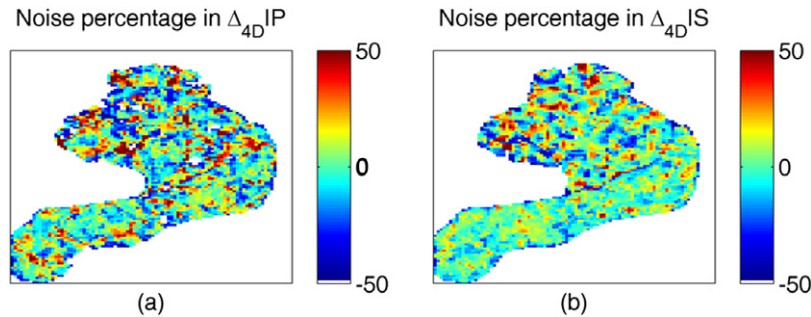


**Figure 5.** Percentage of noise added in the synthetic impedances. (a) Noise percentage in  $\Delta_{4D}IP$  and (b) noise percentage in  $\Delta_{4D}IS$ .

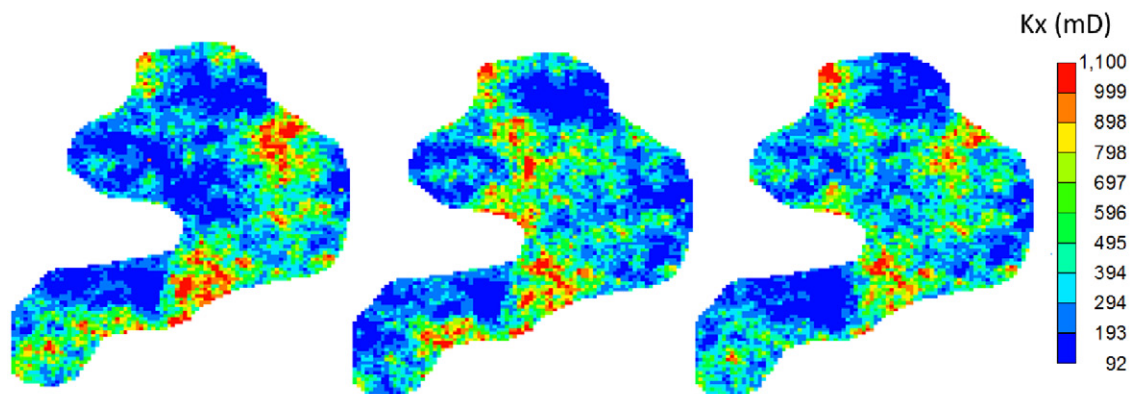


**Figure 6.** Examples of three realizations of permeability.

Figure 7 shows that, even having geostatistical realizations dissimilar to the reference (compare figure 6 with figure 2(b)), the characterization process yielded a good dispersion in the well production curves, i.e., the curves dispersion comprises the history data (figure 7). The top of figure 7 displays the field average pressure and water rate for the 200 models and the history; the bottom of the figure shows the Bottom Hole Pressure (BHP) curves for two wells.

If a poor uncertainty characterization is performed, generating models that do not comprise the history data (e.g. all models below the history curve), the constraints applied to the 4D seismic might lead to biased estimations.

### 3.4. Base model

The base model is the best model among the 200 models realizations generated. It presents the smallest error when

compared to the history curves (pressure and fluid rates for every well).

There are three purposes for choosing a base model: (1) define the porosity field used in equation (1); (2) use its properties, such as porosity, as input to perform the petro-elastic inversion described in section 4.1 and (3) perform the deterministic history matching described in section 4.2. Figure 8 shows the porosity and permeability of the base model.

## 4. Application

The application is divided in two parts. The first discusses how we estimated the Sw maps from 4D seismic data. The second describes the history matching procedure applied here to show the importance of using a calibrated Sw map to update simulation models.

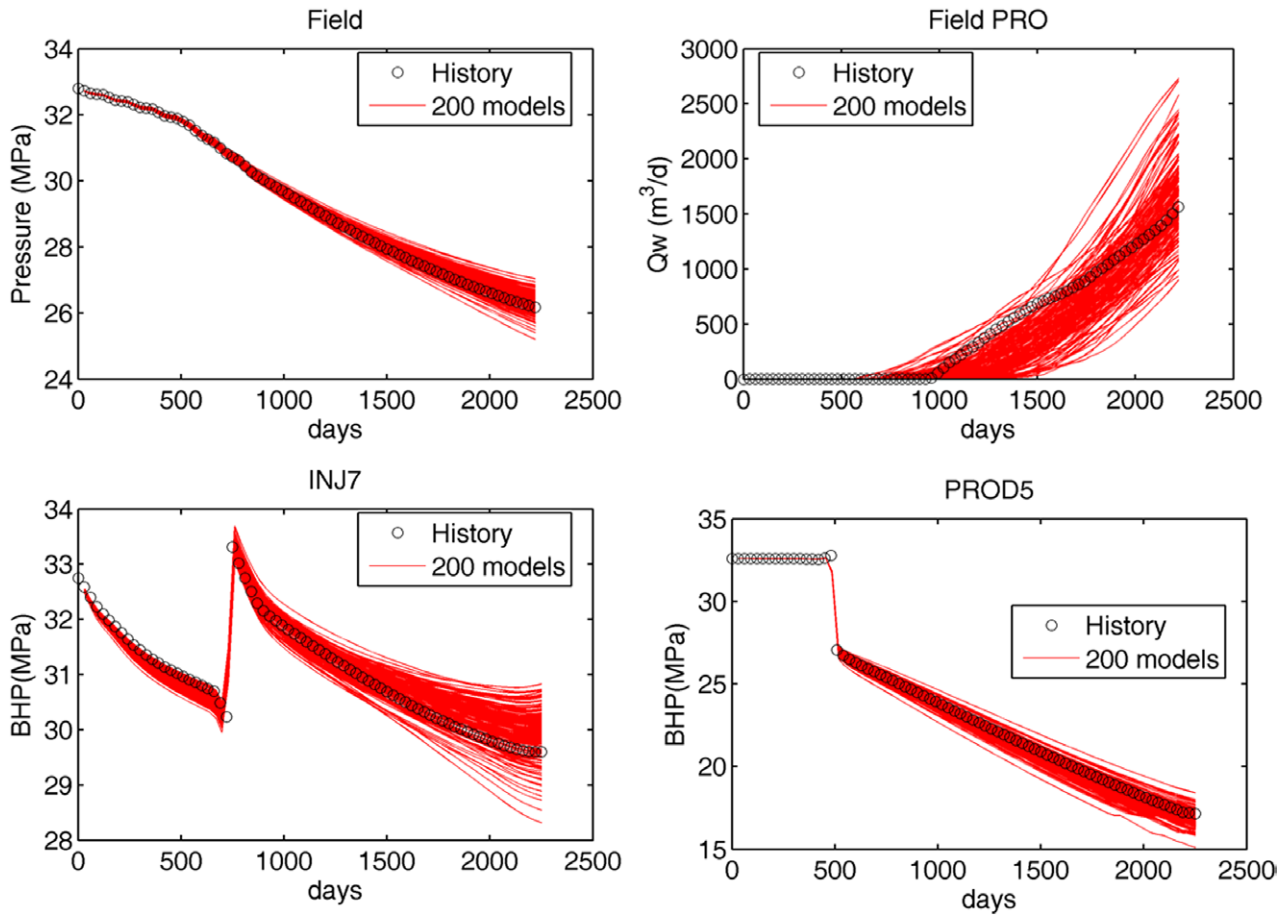


**Figure 7.** Top: field average pressure and field produced water rate. Bottom: examples of bottom hole pressure curves for two wells INJ7 (left) and PROD5 (right).

4.1. Estimating  $S_w$  from 4D seismic data

The water saturation map was estimated using a 4D petro-elastic inversion procedure described in Davolio *et al* [6]. The inversion is done by an optimization process and performed for each simulation block, independently. As discussed in Davolio *et al* [5], this is an optimization problem with only two unknowns (pore pressure and saturation for each block) with a well behaved objective function. So, a gradient-type algorithm is used to search for the solution within the defined search space. The optimization procedure minimizes the difference between observed and computed IP and IS and the results are values of pore pressure and water saturation (we assume no presence of gas) for the monitor survey.

We considered here three error sources for the estimation of P and  $S_w$ : (1) the time-lapse differences of the noisy synthetic P and S impedances (figures 4(c) and (d)), (2) the porosity field extracted from the base model (figure 8(a)) and (3) the overburden pressure which was overestimated by 20% in the inversion. We assumed no errors in the petro-elastic modeling as we used the same model to generate the synthetic impedances as in the inversion process.

The initial pressure and saturations distributions (corresponding to the base survey) are considered known, i.e., with good estimation of the reservoir initial pressure, water-oil contact and capillary pressure. These distributions are used as

input for the inversion but they are kept fixed during optimization, only the dynamic properties of the monitor survey are updated (see Davolio *et al* [5]).

Two inversions were performed to highlight the different steps of calibration of 4D seismic data (INV1 and INV2). It is known that any optimization procedure can have the search space limited to physically feasible ranges. This range definition is the only difference between the two inversions.

A third estimation of saturation (INV2Ca) corresponds to the application of the volume calibration proposed, as described below:

- **INV1:** the inversion procedure is performed with ‘general constraints’, the search space is defined by the limits:  $S_{w_c} < S_w < 1 - S_{o_r}$  and  $P_{prodMin} < P < P_{InjMax}$ .
- **INV2:** the search space is defined by the minimum and maximum values  $[S_{w_{min}}, S_{w_{max}}]$  and  $[P_{min}, P_{max}]$  estimated by the methodology proposed in Davolio *et al* [6] presented in figure 1.
- **INV2Ca:** the calibration of the volume of water is applied to the second saturation map obtained, namely, INV2.

4.2. History matching

The history matching procedure used was proposed by Davolio *et al* [7]. The methodology uses 4D seismic

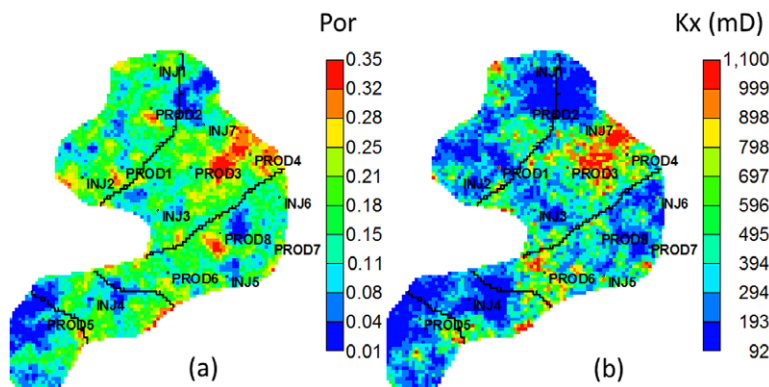


Figure 8. Base model properties of layer 3. (a) Porosity. (b) Horizontal permeability (mD).

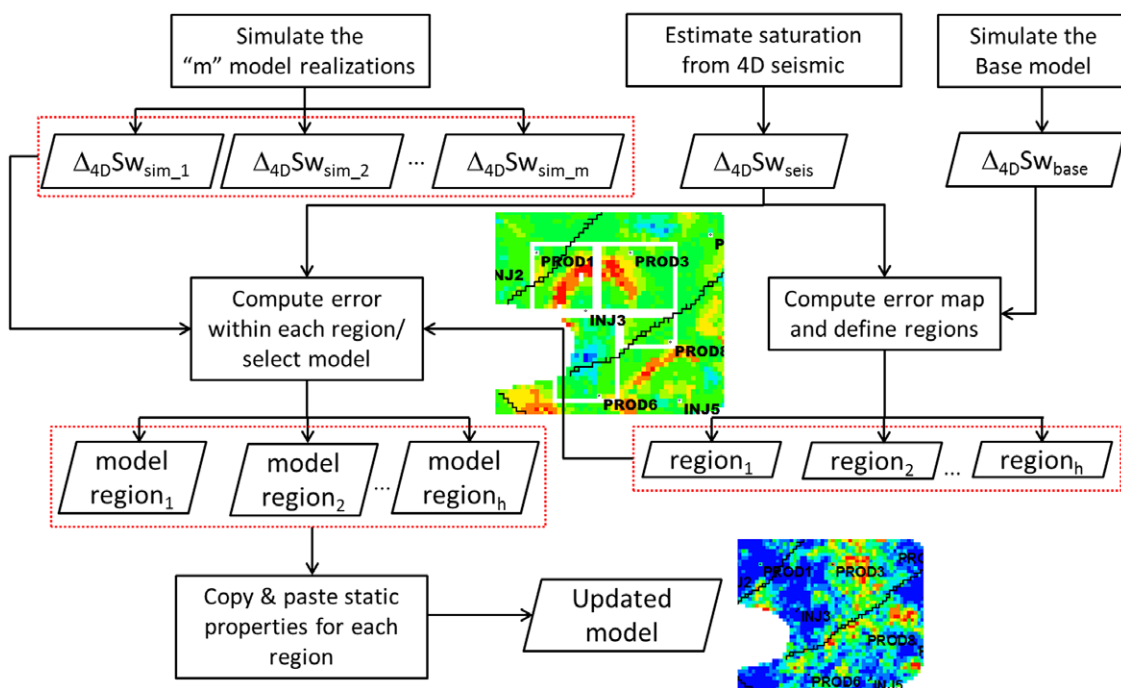


Figure 9. Workflow of the local history matching methodology.

information to run local matching. The water saturation map estimated from 4D seismic data is input to the process to update local properties, namely porosity and permeability, within regions defined around the injector wells. Other input data are several model realizations - the same ‘*m*’ (*m* = 200) models mentioned before (figure 1). The local matching starts by dividing the reservoir into regions according to the location of injector wells and their corresponding water saturation error anomaly (figure 9).

The water saturation error between 4D seismic data and each reservoir model realization is computed within each region. The models with the smallest error for each region are chosen and a new simulation model is built by ‘copying and pasting’ the static properties (porosity and permeability) of selected models in each region, like patchwork.

As stated in Davolio *et al* [7], this procedure does not ensure that the updated model is geostatistically consistent, but this is not an issue here because the procedure is used only to compare the differences of the history matched model when different inputs from 4D seismic are used. Thus, the quality of the matching and the updated model is not an issue.

The history matching procedure was performed three times. The only difference among them is the input Sw map:

- LHM1** = local history matching using as input the estimated Sw map from INV1;
- LHM2** = local history matching using as input the estimated Sw map from INV2;
- LHM3** = local history matching using as input the estimated Sw map from INV2Ca.

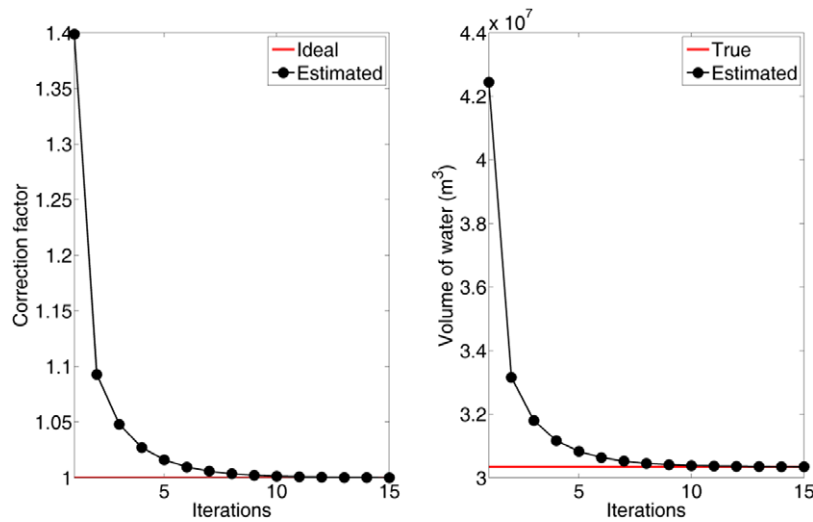


**Figure 10.** Fifteen iterations of the proposed volume calibration procedure (steps 2–9 in section 2). Left: the correction factor computed per iteration. Right: the calibrated volume of water per iteration.

## 5. Results

### 5.1. Estimating Sw from 4D seismic data

The volume calibration methodology was applied to the whole reservoir, meaning that all the correction factor calculations considered the volume of water present in the entire reservoir.

As mentioned in section 2, steps 2–9 of the volume calibration proposed are repeated until  $CF - 1 < \text{tolerance}$ . In this work, 15 iterations were enough to reach a good calibration. Figure 10 shows the performance of the volume calibration. The iterations correspond to steps 2–9. The first correction factor computed was:  $CF = (4.24 \times 10^7) \text{ m}^3 / (3.03 \times 10^7) \text{ m}^3 \approx 1.4$ . After the first iteration, the calibrated volume was  $\approx 3.32 \times 10^7 \text{ m}^3$ . This new volume yielded a  $CF \approx 1.09$ . After applying this second CF, the new volume was  $\approx 3.18 \times 10^7 \text{ m}^3$  and so on until the 15th iteration that yielded a satisfactory calibration of  $CF - 1 = 10^{-4}$ .

The sizable correction factor computed for the dataset used comes from the three sources of error present in the estimation of the saturation map: porosity field, noise added to the impedances and overestimation of overburden pressure.

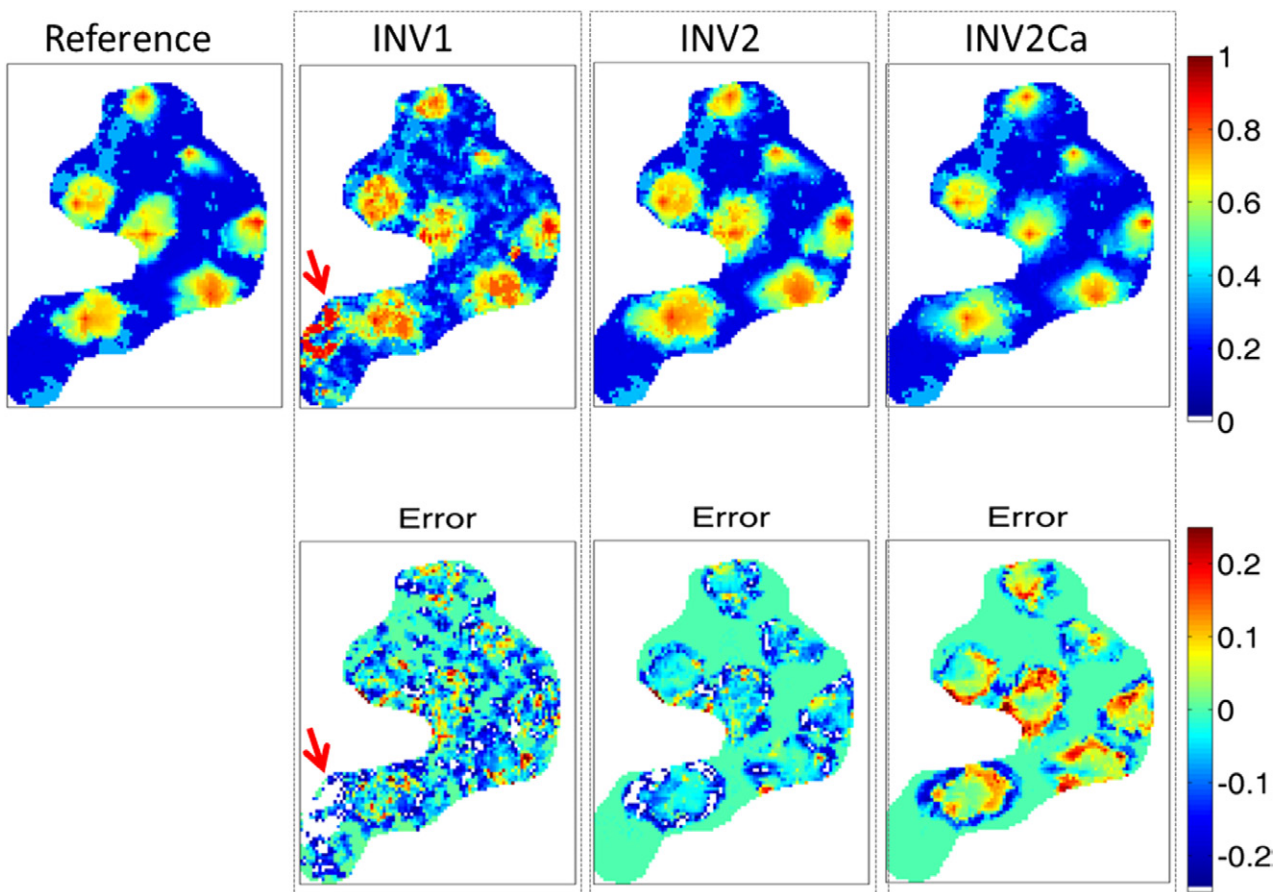
Figure 11 shows the estimated water saturation maps for the three inversions and the water saturation map yielded from the simulation of the reference model, which represents the answer that the inversions aim to reach. The same figure shows the respective error map of the three inversion results; the error is the difference between the reference map and the estimations. Due to the noise added to seismic impedances and the wrong porosity used as inputs for the petro-elastic inversion, the results of INV1 presented a noisy aspect clearly seen in the error map. A zone with high errors is indicated by a red arrow; the white region in the error map shows out-of-scale error (bigger than 0.2). The poor characterization of porosity in that region (compare figures 2(a) and 8(a)) was the main cause of this error.

Figure 12 follows the same layout of figure 11 but shows the estimates of pressure for INV1 and INV2; the noisy behavior of INV1, previously mentioned for Sw, is seen in pressure as well. Similarly, the region with the highest errors marked in the Sw map also presents a high error for pressure.

When the estimation of Sw is constrained to flow conditions (INV2), an error reduction is seen in figure 11. The use of constraints corrected some areas that had been incorrectly estimated due to seismic noise. Also, the region with high errors observed in INV1 now presents a more accurate response. This is because the constraints applied to the search space ‘forced’ the dynamic properties estimations (saturation and pressure) to more physically consistent values, reducing the effects of wrong static properties characterization. The same improvement can be observed in the estimation of pressure for INV2 (figure 12). The strong error reduction between INV1 and INV2 observed in figure 12 was ensured by the proper mapping of uncertainties, which generated model realizations with pressure behaviors that closely follow history data, as verified in figure 7.

Although the result of INV2 presented a water saturation map closer to the reference, the error anomalies are mainly negative, meaning that the estimated water saturation presents more water than the reference model, showing the need to calibrate the volume of water. As in practice, these errors are not available information, this could be checked by a computation of the volume of water (equation (1)) and comparison with the known volume of injected water in reservoir conditions.

After applying our proposed volume calibration (INV2Ca), the injection anomalies are better defined and present unbiased values. The observed error indicates that the mass balance is respected, as it presents positive and negative anomalies, meaning that the error is now more related to an incorrect water front displacement and not with the amount of water.



**Figure 11.** Water saturation maps of layer 3 for the second production time (monitor survey). Top: from left to right, the reference model (answer), the estimated Sw map for cases 1–3. Bottom: from left to right, the error (reference—INV) for the three estimations.

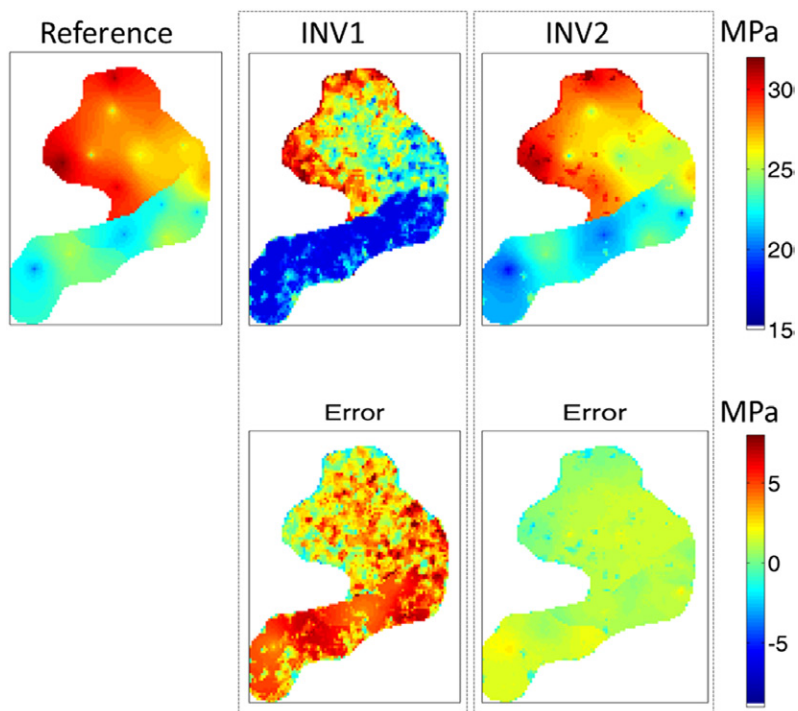


**Figure 12.** Pore pressure maps of layer 3 for the second production time (monitor survey). Top: from left to right, the reference model (answer), the estimations of INV1 and INV2. Bottom: from left to right, the error (reference—INV) for the two estimations.

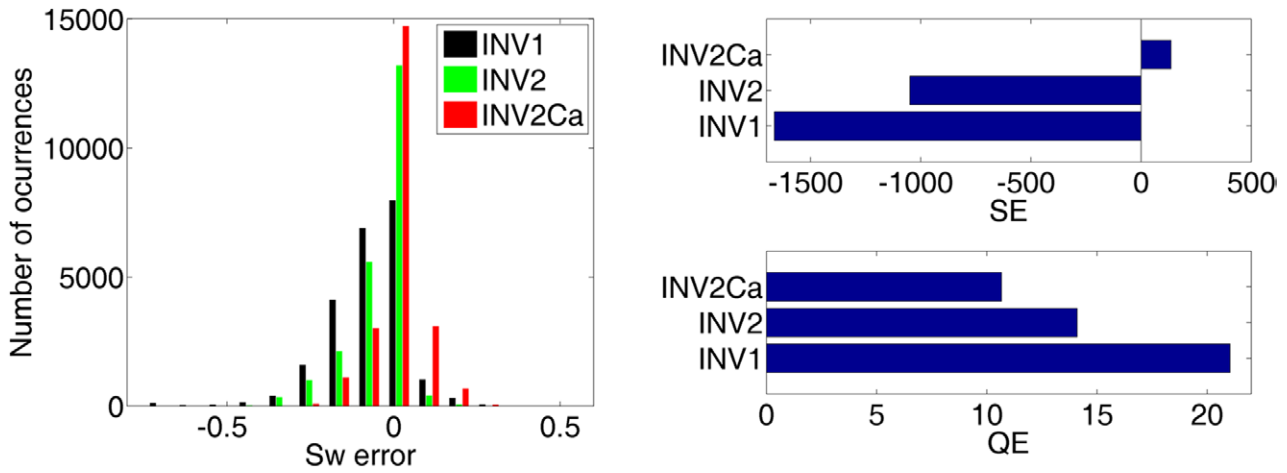


**Figure 13.** Statistics of the Sw errors displayed in the bottom of figure 11. Left: histogram of the Sw error. Right: graph of the simple Sw error (equation (7)) and quadratic Sw error (equation (8)).

Figure 13 shows statistics of Sw errors seen in the bottom of figure 11. The bar graphs show the simple error (SE) and the quadratic error (QE) given by the equations,

$$SE = \sum_{i=1}^{nb} (\text{reference} - \text{estimated}) , \quad (7)$$

$$QE = \sum_{i=1}^{nb} (\text{reference} - \text{estimated})^2 , \quad (8)$$

in this figure, the variables *reference* and *estimated* correspond to Sw values of the reference model and those obtained from the inversions. The bar graph shows the error reduction seen from INV1 to INV2 and INV2Ca. The histogram shows that for INV2Ca, the errors are centralized at zero, with some positive and negative values, indicating that the amount of water present in the estimated map is more balanced than in the other two cases.

### 5.2. History matching

To perform the local history matching, we first define areas based on the observed Sw error and the location of injector wells; figure 14 defines these regions. We selected injector wells with the highest errors (for all layers) to perform the local match: INJ1, INJ3, INJ4 and INJ5 (see Davolio et al [7] for details about region definition).

The estimated Sw of INV2 (figure 11) was used to compute the error map shown in figure 14, which is the same input used to define the regions in Davolio et al [7]. As mentioned, the local matching procedure in section 4.2 was performed for three cases (LHM1, LHM2 and LHM3), the difference was the Sw map used as input. Although region definition is dependent on the input data, in this work, the regions shown below were used for the three history matching, to compare results.

Figure 15(a) shows the Sw error map (compared to the true answer) of the base model before local matching. Figures 15(b)–(d) show error maps for the three updated

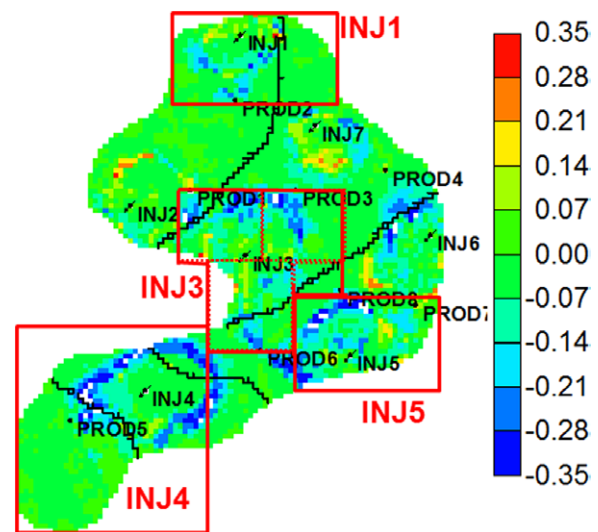


**Figure 14.** Water saturation error map ( $\Delta_{4D}Sw_{base} - \Delta_{4D}Sw_{seis}$ ) with the regions defined to perform the local matching.

models. The updated models LHM1 and LHM2 show more water than they should; see the predominance of negative anomalies. These results are because the matching procedure updates static properties to match the Sw maps of INV1 and INV2, displayed in figure 11, which also show more water.

Figure 16 shows the saturation error (compared to the Sw map estimated from 4D seismic data) for each case, before and after the matching; these images indicate the quality of the procedure. The matching procedure worked for LHM1 and LHM2, i.e., the updated models provided Sw maps closer to the observed in 4D seismic data; see the error reduction from the top images to the bottom ones. However, these results are unsatisfactory, since the two matching processes increased the saturation errors when compared to the true results, as shown in figures 15(b) and (c).

The quantitative use of estimated Sw from 4D seismic data was successful in the third history matching (LHM3). Figure 15(d) shows a decrease in the Sw error when compared to figures 15(b) and (c). However, some errors are still

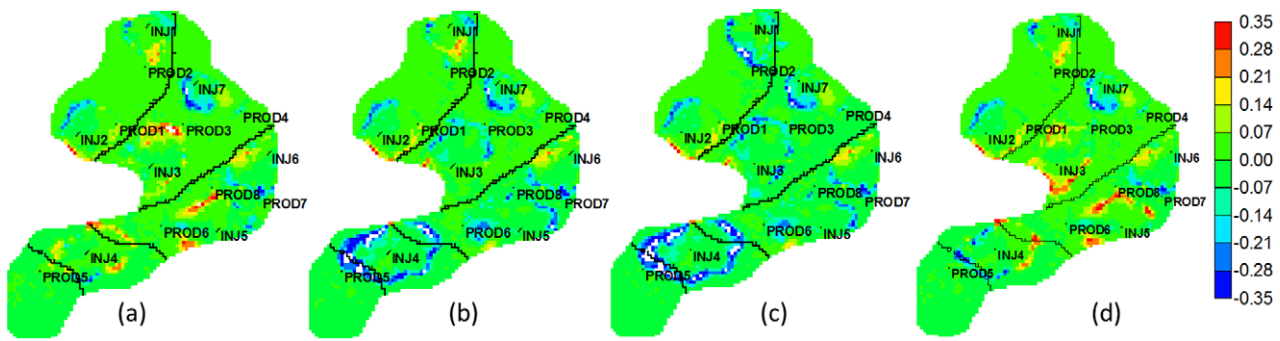


Figure 15. Water saturation error map of layer 3 (reference—simulated) of the base model before (a) and after the local matching LHM1 (b), LHM2 (c) and LHM3 (d).

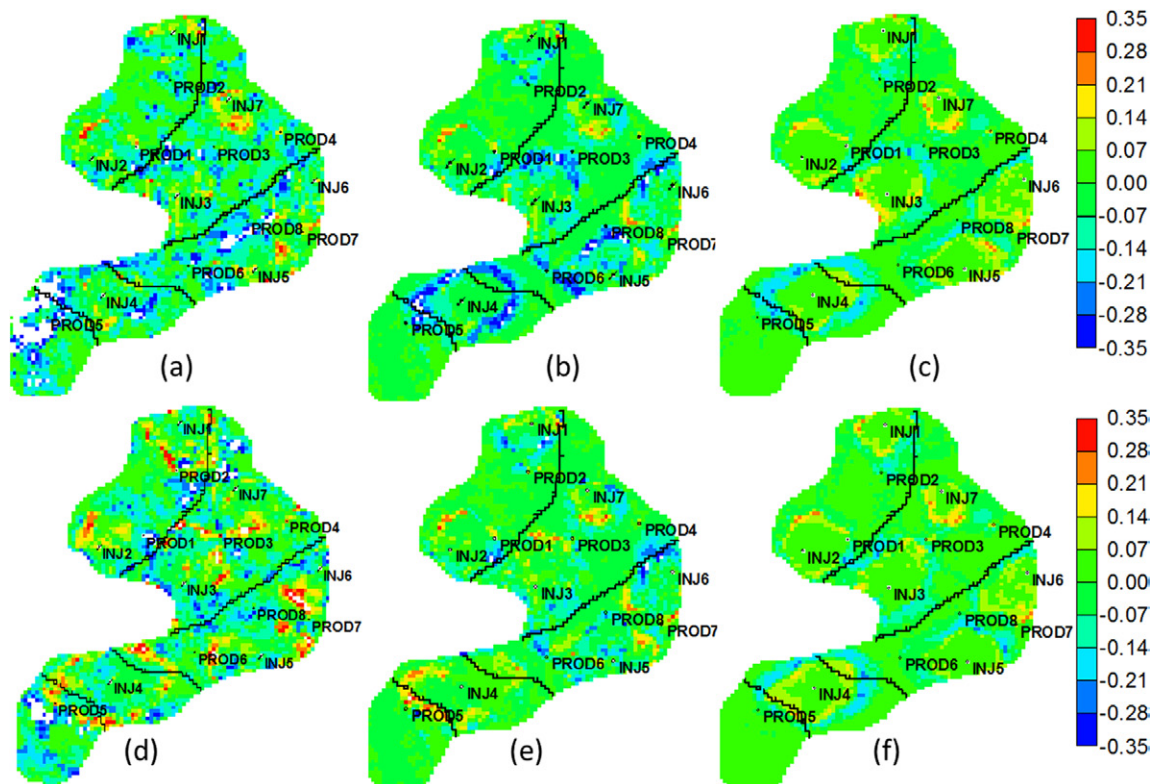


Figure 16. Observed water saturation error map (estimated from 4D seismic—simulated). Top: difference between the estimated saturation INV1(a), INV2 (b) and INV2Cal (c) and the saturation of the base model before the matching. Bottom: difference between the estimated saturation INV1 (d), INV2 (e) and INV2Cal (f) and the saturation of the base model after the respective history matching (LHM1, LHM2 and LHM3).

observed for this case for two reasons: (1) although better calibrated, the map IN2Cal still carries errors and (2) the characterization process is not assumed to be perfect, i.e., the image realizations of porosity and permeability do not reproduce the reference properties.

The graphs in figure 17 show the simple Sw errors (equation (7)) and the quadratic Sw errors (equation (8)) for the three cases; in this figure, the variables *reference* and *estimated* correspond to Sw values of the reference model and those obtained from the simulation of the three history matched models. The cumulative error displayed in figure 17 shows that LHM3 presents a better error balance with positive and negative values. In the same figure, the 2-norm of the errors indicates that LHM3 has the best result.

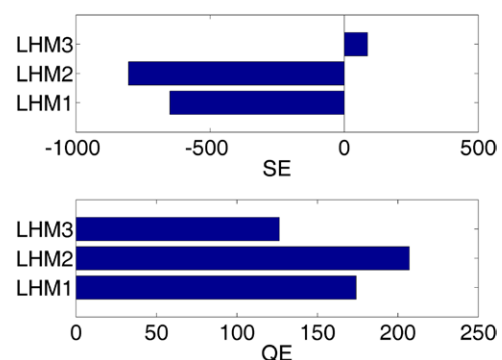


Figure 17. Simple (top) and quadratic (bottom) errors of the Sw error map for the three history matching applied.

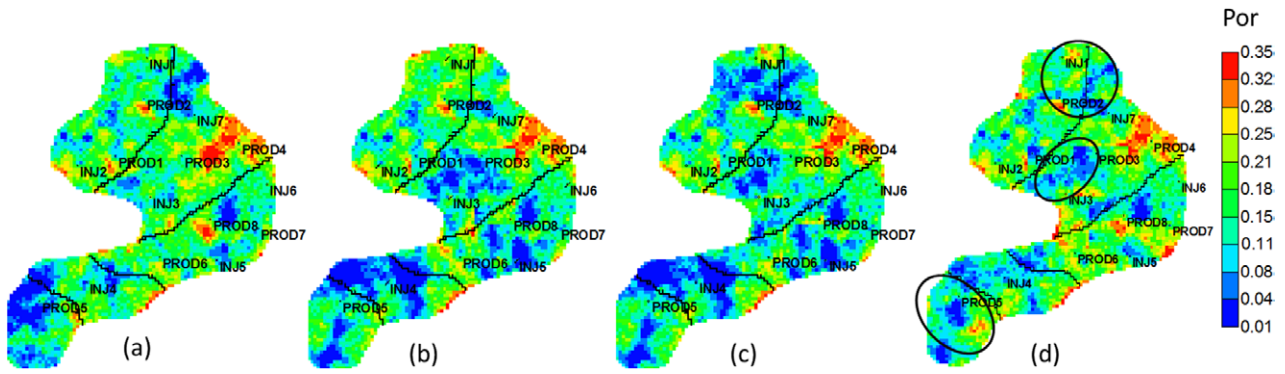


Figure 18. Porosity field of the base model before (a) and after the local matching LHM1 (b), LHM2 (c) and LHM3 (d). Layer 3.

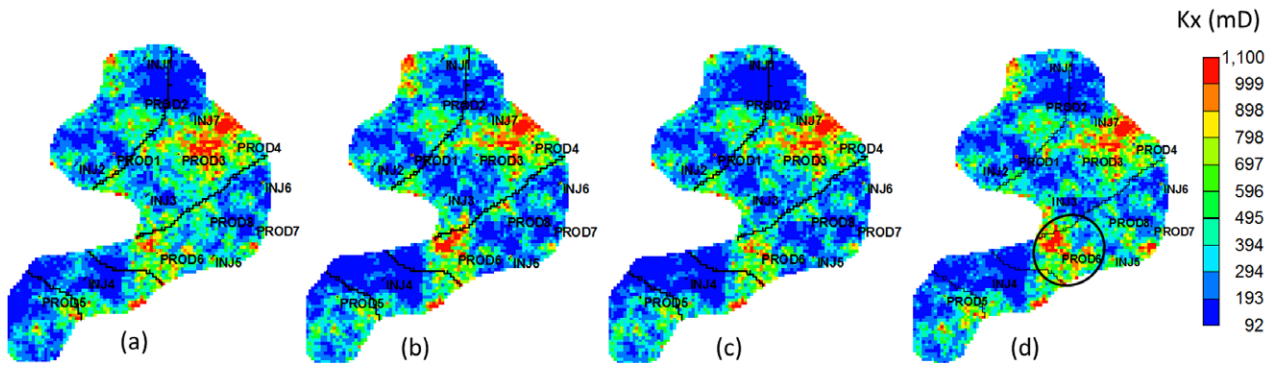


Figure 19. Horizontal permeability field of the base model before (a) and after the local matching LHM1 (b), LHM2 (c) and LHM3 (d). Layer 3.

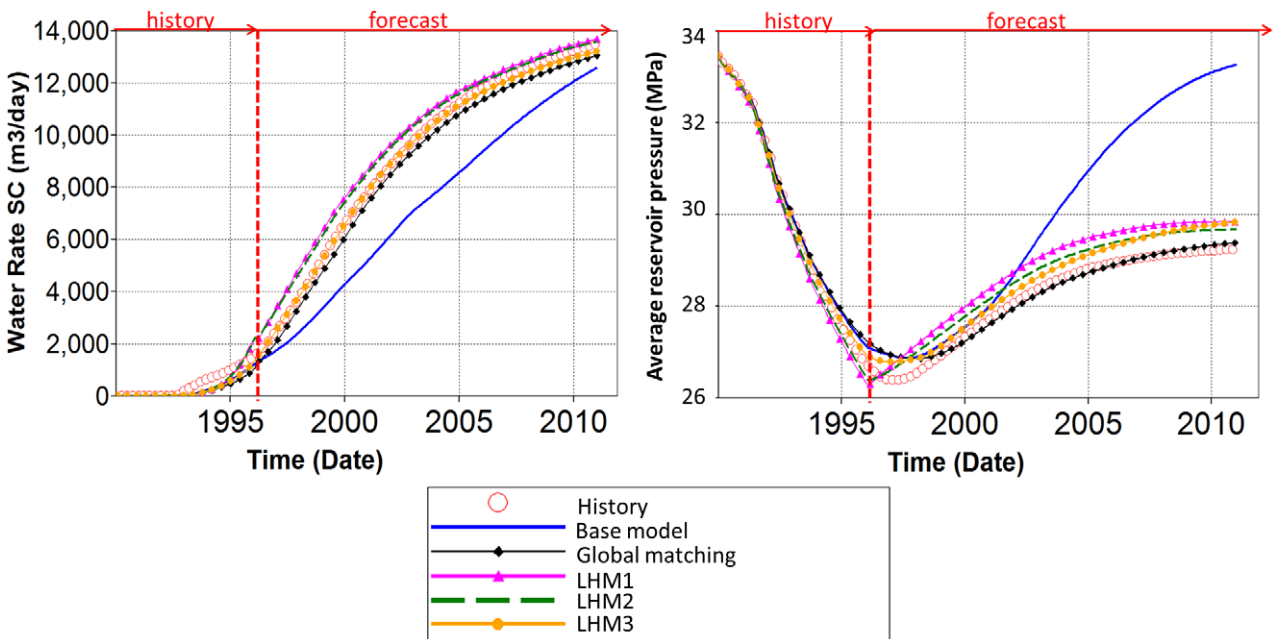
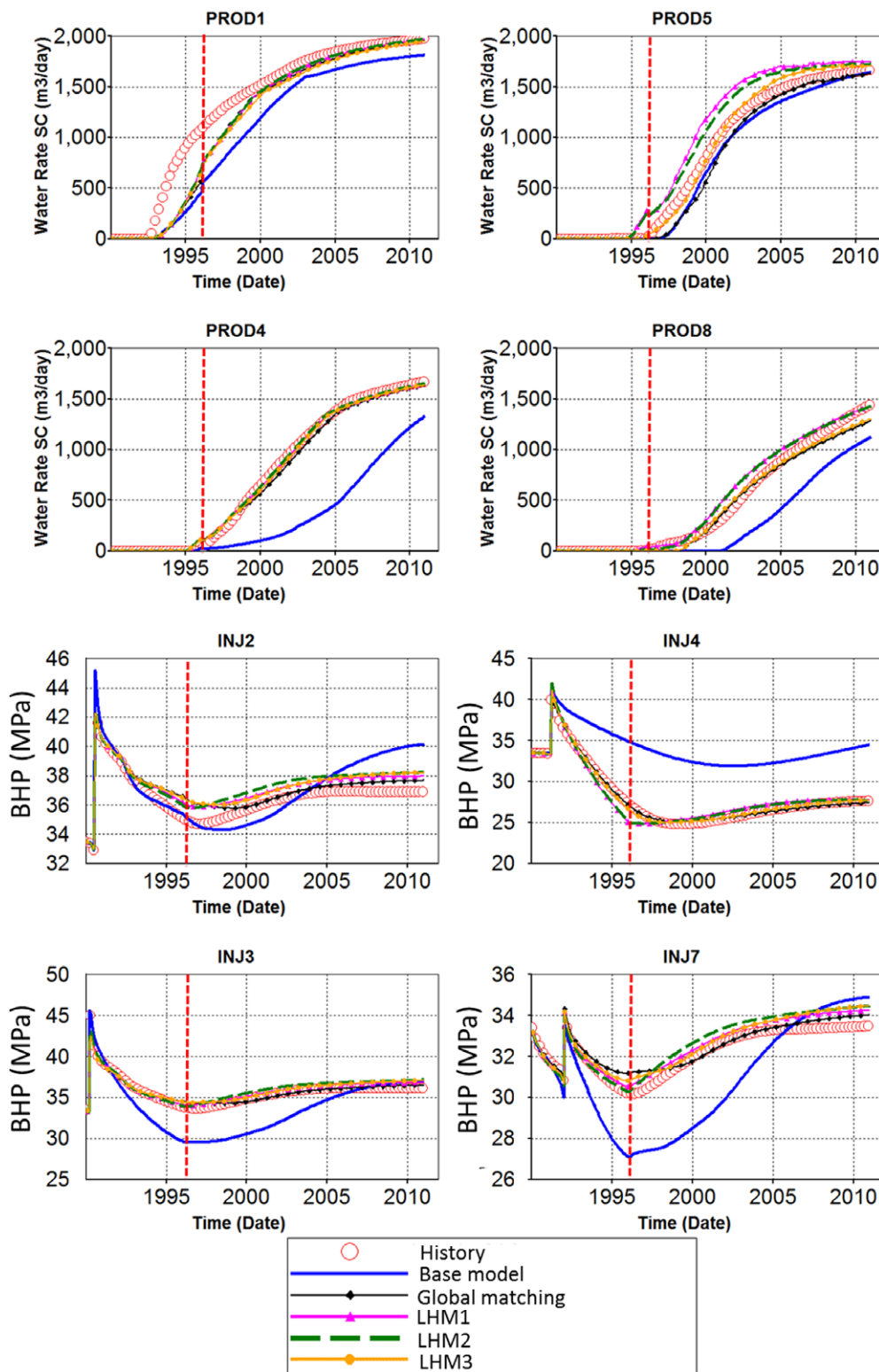


Figure 20. Field water rate and average pressure. The vertical line divides the period of time into two: history and forecast.

One can say that the base model before the matching (figure 15(a)) presents the same amount of errors as LHM3 (figure 15(d)). Indeed, there is a slight error reduction in the Sw map after the local matching LHM3. This could be improved, for instance, by re-defining the regions according to observed

error anomalies specific to this case, or by improving the characterization process (changing the geostatistical parameterization). However, the focus of this work is not to guarantee the best history matching result but to analyze the importance of having better input information to do so. In this sense, the



**Figure 21.** Well water rate and bottom hole pressure for some wells. The vertical line divides the period of time into two: history and forecast.

results of figures 15 and 17 demonstrated that the use of the calibrated water saturation map (LHM3) is the most reliable option.

The updated porosity field after the matching process LHM3 has more similar structures to the reference model than the base model and the other two matches (figure 18). The

regions marked in figure 18(d) are examples of good agreement with the reference porosity field displayed in figure 2(a). A less pronounced improvement for permeability is observed (figure 19), because the characterization process of permeability needs to be improved, since the image realizations (figure 6) do not present the expected features seen in figure 2(b).

Even so, figure 19(d) highlights a better definition of a high permeability zone.

Figures 20 and 21 show the production curves for the field and some of the wells comparing the history matching performances. Of note are the accurate field water rate forecast yielded from LHM3 and the good field pressure behavior in the history period for the same model. The main improvement observed is from the initial base model to the model after global matching. Then, small changes are observed between the models after global matching and after local matching (LHM1, LHM2 and LHM3), showing that the second procedure has not changed the quality of the first.

## 6. Final remarks

The results presented here show that it is possible to use reservoir simulation data to reduce errors in the estimation of dynamic changes from 4D seismic data. The addition of engineering information helps to lessen the effects of poor static properties characterization and seismic signal problems. For the history matching process, the results show that the calibration of input data is important to update reservoir models, namely LHM3 provided the best result when compared to the other two history matching.

We applied our proposed methodology to calibrate the volume of water in a synthetic dataset. In this dataset, the Sw map provided by 4D seismic presented more water than expected for the entire reservoir. However, the volume calibration and the history matching were built to be performed locally. For more complex cases, some regions of the reservoir may present a volume bigger or smaller than expected. In these cases, the correction factor that was computed and applied here to the entire reservoir can be computed/applied individually for each region of interest. In this case, there would be an additional step: identifying the water anomalies associated with each injector well to compute individual volumes for each injector.

## 7. Conclusions

We proposed a methodology to calibrate the volume of water associated with water saturation maps provided by 4D seismic data. The volume calibration is made based on reservoir flow conditions imposed by the simulation of several models. As these models account for mapped uncertainties, the calibrated water saturation map is consistent with flow conditions resulting from the stage of characterization of the reservoir. This process can be repeated whenever new information is available (e.g.: after a new run of a history matching).

The advantages of applying the proposed methodology were shown in two forms: (1) comparing the water saturation maps estimated from a petro-elastic inversion process, with and without the volume calibration, and (2) comparing the results of a history matching procedure that uses the estimated water saturation maps to update local static properties.

Synthetic data was used in both cases to validate the methodology and as for the main results we highlight: (1) calibrated water saturation maps provided more reliable information (to be used qualitatively or quantitatively), as it is more physically consistent (respecting the mass balance); (2) the use of calibrated water saturation maps in a history matching is important to ensure that static properties be properly updated.

## Acknowledgments

The authors would like to thank UNISIM, BG, PETROBRAS, CEPETRO and the Department of Petroleum Engineering for supporting this work. We also thank CMG and Schlumberger for software licenses.

## References

- [1] Batzle M and Wang Z 1992 Seismic properties of pore fluids *Geophysics* **57** 1396–408
- [2] Castro S A, Caers J, Otterlei C M, Meisingset H, Hoye T, Gomel P and Zachariassen E 2009 Incorporating 4D seismic data into reservoir models while honoring production and geologic data: a case study *Leading Edge* **28** 1498–506
- [3] Brito D, Moraes R and Emerick A 2010 The Marlim field: incorporating time-lapse seismic in the assisted history matching SPE137763 *SPE Latin American & Caribbean Petroleum Engineering Conf.* (Lima December 2010)
- [4] Dadashpour M, Landrø M and Kleppe J 2008. Nonlinear inversion for estimating reservoir parameters from time-lapse seismic data *J. Geophys. Eng.* **5** 54–66
- [5] Davolio A, Maschio C and Schiozer D J 2012 Pressure and saturation estimation from P and S impedance: a theoretical study *J. Geophys. Eng.* **9** 447–60
- [6] Davolio A, Maschio C and Schiozer D J 2013 A methodology to constrain pressure and saturation estimation from 4D seismic using multiple simulation models and observed data *J. Petroleum Sci. Eng.* **105** 51–61
- [7] Davolio A, Maschio C and Schiozer D J 2013 Local history matching using 4D seismic data and multiple models combination SPE164883 *SPE EUROPEC/EAGE Ann. Conf. Exhibition* (London, June 2013)
- [8] Emerick A A and Reynolds A C 2012 History matching time-lapse seismic data using the ensemble Kalman filter with multiple data assimilations *Comput. Geosci.* **16** 639–59
- [9] Gosselin O, Aanonsen S I, Aavatsmark I, Cominelli A, Gonard R, Kolasinski M, Ferdinandi F, Kovacic L and Neylon K 2003. History matching using time-lapse seismic (HUTS) SPE 84464 *Ann. Tech. Conf. Exhibition* (Denver, October 2003)
- [10] Huang Y, MacBeth C, Barvked O, Gestel J P V and Dybvik O P 2011 Enhanced dynamic interpretation from correlating well activity to frequently acquired 4D seismic signatures *Leading Edge* **30** 1042–50
- [11] Johann P, Sansonowski R, Oliveira R and Bampi D 2009 4D seismic in a heavy-oil turbidite reservoir offshore Brazil *Leading Edge* **28** 718–29
- [12] Jin L, Alpak F O, van den Hoek P, Pirmez C, Fehintola T, Tendo F and Olaniyan E E 2011 A comparison of stochastic data-integration algorithms for the joint history matching of production and time-lapse seismic data SPE 146418 *Ann. Tech. Conf. Exhibition* (Denver, October–November 2011)
- [13] Lake L W 1989 *Enhanced Oil Recovery* (Englewood Cliffs: Prentice Hall) pp 61–2

- [14] Landa J L and Horne R N 1997 A procedure to integrate well test data, reservoir performance history and 4D seismic information into a reservoir description SPE 38653 *Ann. Tech. Conf. Exhibition* (San Antonio, October 1997)
- [15] Landa J L and Kumar D 2011 Joint inversion of 4D seismic and production data *SPE Tech. Conf. Exhibition* (Denver, October–November 2011)
- [16] Landro M 2001 Discrimination between pressure and fluid saturation changes from time-lapse seismic data *Geophysics* **66** 836–44
- [17] Lumley D, Adams D, Meadows M, Cole S and Ergas R 2003 4D seismic pressure-saturation inversion at Gullfaks field, Norway *First Break* **21** 49–58
- [18] MacBeth C, Floricich M and Soldo J 2006 Going quantitative with 4D seismic analysis *Geophys. Prospect.* **54** 303–17
- [19] Mavko G, Mukerji T and Dvorkin J 2003 *The Rock Physics Handbook: Tools for Seismic Analysis in Porous Media* (Cambridge: Cambridge University Press)
- [20] Skjervheim J A, Evensen G, Aanonsen S I, Ruud B O and Johansen T A 2007 Incorporating 4D seismic data in reservoir simulation models using ensemble Kalman filter *SPE J.* **12** 282–92
- [21] Stephen K D, Soldo J, MacBeth C and Christie M 2006 Multiple model seismic and production history matching: a case study *SPE J.* **11** 418–30
- [22] Tolstukhin E, Lyngnes B and Sudan H H 2012 Ekofisk 4D seismic–seismic history matching workflow SPE154347 *EUROPEC/EAGE Ann. Conf. Exhibition* (Copenhagen, June 2012)
- [23] Toinet S, Maultzsch S, Souvannavong V and Volnard O 2011 4D pre-stack inversion workflow integrating reservoir model control and lithology supervised classification *Fisrt Break* **29** 59–66
- [24] Tuttle C, Pelissier M, Barnes M, Tribe J and Persad K 2009 A seismically constrained reservoir modeling workflow: case study *Leading Edge* **28** 1492–7